

Nerve Fiber Segmentation from Microscopic Cross Sections Based on Spatially Constrained Registration Strategy

^{1,4}Hsin-Chen Chen, ²Yi-Ying Wang, ³Chou-Ching K. Lin and ^{1,*}Yung-Nien Sun

Abstract

Segmentation of myelinated nerve fiber cross sections (MNFC) from a sequence of microscopic cross-sectional images, which can be used to construct the three-dimensional (3D) structure of nerve fiber, is important for evaluating neurological disorders and nerve regeneration. However, most existing segmentation methods do not take the spatial relationships between inter-frame MNFCs into account, so they usually suffer from several difficulties, such as large intensity variations among frames and blurred MNFC boundaries, in obtaining desirable segmentation results. In this paper, we propose a new segmentation method based on spatially constrained registration (SCR) to automatically segment and reconstruct the 3D structure of nerve fiber from microscopic images. At first, we utilize a multi-scale gradient watershed-based segmentation algorithm to segment the MNFCs from each image frame. Considering the continuity of the 3D fiber structure, the MNFC contexts between adjacent frames are supposed to be dependent. The SCR strategy is then employed to assure the connectivity between the adjacent MNFCs. Based on the connectivity we subsequently recover the missing MNFCs with a compensation mechanism and finish the segmentation process. Two sets of rat tibia nerve images (45 nerve fiber cross-section patches) were used to validate the accuracy of the proposed method. Experiments showed that our method can overcome the aforementioned difficulties and achieve satisfactory segmentation results. The experiments also demonstrated that the proposed SCR method established more reliable correspondences of MNFCs over the conventional iterative closest point (ICP) registration algorithm.

Key words: fuzzy rules; iterative closest point; nerve fiber reconstruction; spatially constrained registration; Voronoi diagram; watershed

*Corresponding Author: Yung-Nien Sun
(E-mail: ynsun@mail.ncku.edu.tw)

¹Department of Computer Science and Information Engineering, National Cheng Kung University, 1 University Road, Tainan 701, Taiwan

²Hermes Microvision Inc., 7F., No.18, Puding Rd., East Dist., Hsinchu City 300, Taiwan

³Department of Neurology, Medical Center, National Cheng Kung University, Tainan, 701, Taiwan

⁴Department of Radiation Oncology, Washington University, Saint Louis, MO 63110, USA

1. Introduction

The three-dimensional (3D) reconstruction of nerve fiber can provide an important structural information for assessing neurological diseases, nerve repair and regeneration. To reconstruct the nerve structure, segmentation of myelinated nerve fiber cross sections (MNFC) from a sequence of microscopic images is the most critical step because it greatly influences the reconstruction accuracy. However, few studies have discussed the issue of automatic MNFC segmentation. Since the context in MNFC images is comparable with some cell images, segmentation methods for nerve fiber and cell images were both addressed below [1-11]. Yousef et al. [1] proposed a hybrid method to segment cell nuclei. First, a graph cuts-based binarization was used to extract the foreground from the images. Next, a method combining a multi-scale Laplacian of Gaussian filter was applied to detect nuclear seed points. Using these points to perform an initial segmentation, the result was further refined by another graph cuts-based algorithm. Cheng et al. [3] presented a method to segment nuclei from fluorescence microscopic images. A level set evolution method was first used to detect the initial positions of nuclei, and then a marker-controlled watershed algorithm was hired to separate the clustered nuclei. In addition, our previous work [4] investigated the multi-scale gradient watershed hierarchies in order to segment MNFCs from microscopic cross-sectional images of nerve fibers. Although good segmentation accuracy was achieved, there were still some mis-detected MNFCs on the microscopic images. Overall, the above-mentioned methods were designed to segment cells or MNFCs from a single image frame. Since artifacts of specimen slicing or imaging may yield vague boundaries and/or irregularly distributed intensities of subjects in the acquired images, the single-frame segmentation methods which do not take the spatial relationship between inter-frame MNFCs into account are weak in handling these image artifacts.

Rigid registration is commonly used to correlate two images by the use of an optimal geometric transformation. With the aid of registration, several registration-assisted segmentation methods have been proposed to improve the segmentation results from different image modalities [12-16].

Gorthi et al. [14] used an active contour-based atlas registration model to segment the lymph node regions. Their model combined the dense deformation field between two structures with local segmentation constraints via an active contour segmentation framework. Chen et al. [15] proposed a registration-based method to automatically segment hand bones with an articulated model from multi-postural MR images. Zagrodsky et al. [16] also presented a registration-assisted method to segment the cardiac surface from 4D echocardiographic data and then visualized it at different phases of the cardiac cycle. However, to date there is still no efficient registration-based method for segmenting a large number of cells or MNFCs from

The iterative closest point (ICP) registration [17] is a popular method for aligning two point sets due to its simplicity in implementation and efficiency in convergence. The ICP alternates two steps, one of which is intended to identify the point correspondences by the nearest points, and the other of which is to calculate the Euclidean distances between all pairs of corresponding points. Such an iterative optimization procedure continues until the sum of the Euclidean distances is minimized. However, since the ICP only utilizes the Euclidean distance as the registration feature, it may yield many-to-one or one-to-many correspondences during the registration process, resulting in a tendency for the ICP to be stuck in undesirable local solutions [18]. Thus, there were some reports trying to improve the performance of the ICP algorithm by adding additional features into the registration function for the purpose of establishing more proper correspondences between source and target points. Rogers et al. [19] adopted several features including the Euclidean distance, shape context, spot size and intensity to estimate the correspondences for point matching. Sharp et al. [20] investigated a feature-based ICP registration approach on range images, in which the selection of correspondences was based on the weighted linear combination of position and feature distances. However, incorrect decisions on correspondences may be made due to the lack of suitable weights to integrate these features. Determining a method by which to combine these features in order to obtain proper correspondences thus becomes an important issue.

Fuzzy inference, which is a way of formalizing the reasoning process of human language, is frequently adopted to solve the aforementioned decision problem. Chung et al. [21] proposed a fuzzy rule-based method to model the variations of geometric transformations and features for elastic image registration. Kobashi et al. [22] proposed a fuzzy rule-based active contour and surface models to divide the cerebrum into cerebral lobes. Also, Chen et al. [23] handled nonlinear shape distortions in fingerprint images based on fuzzy theory. Although these studies do not present a direct solution to the

automatic registration of cells or MNFCs, they give us inspiration leading to a supposition that the fuzzy inference system may be an efficient technique to integrate multiple registration features for establishing point correspondences.

In this paper we propose a new registration-based method to automatically segment and reconstruct the 3D structure of nerve fiber from a sequence of microscopic cross-sectional images. The major features of the proposed method are described below. At first, we incorporate the biological knowledge of nerve fiber structure to design the spatially constrained registration (SCR) strategy in order to efficiently correlate inter-frame MNFCs. Moreover, compared to the conventional iterative closest point (ICP) method, the proposed method can establish more reliable correspondences of MNFCs by incorporating multiple MNFC geometric features in the registration process. In addition, we employ fuzzy logic to properly integrate these features for the purpose of assuring the correspondence of MNFCs between adjacent frames. At last, we develop a compensation mechanism based on inter-frame MNFC connectivity to improve the segmentation of MNFCs with missing cross sections. After the MNFCs of all microscopic images are segmented, the 3D structure of nerve fiber can be reconstructed and visualized. The proposed method is near fully automatic and able to yield reproducible segmentation results from microscopic data sets.

2. Image Preparation and Description

The nerve fiber cross-sectional images in the present study were acquired from serially sliced frozen specimens of rat tibia nerves. A typical nerve fascicle cross section is outlined with the black thick contour in Fig. 1(a). In general, the structure of a MNFC can be specified by an axon (indicated by arrow 1) and its surrounding myelin sheath (indicated by arrow 2), and a large collection of MNFCs constitutes a nerve fascicle. Due to natural endoneurial spaces in the nerve fiber (indicated by arrows 3-5), the nerve fascicle in a microscopic cross-sectional image is usually divided into several sub-fascicles, as indicated by the black contours in Fig. 1(b). Such a biological phenomenon of nerve fiber structure, which is helpful for the registration of nerve fiber in microscopic images, is adopted in the proposed method.

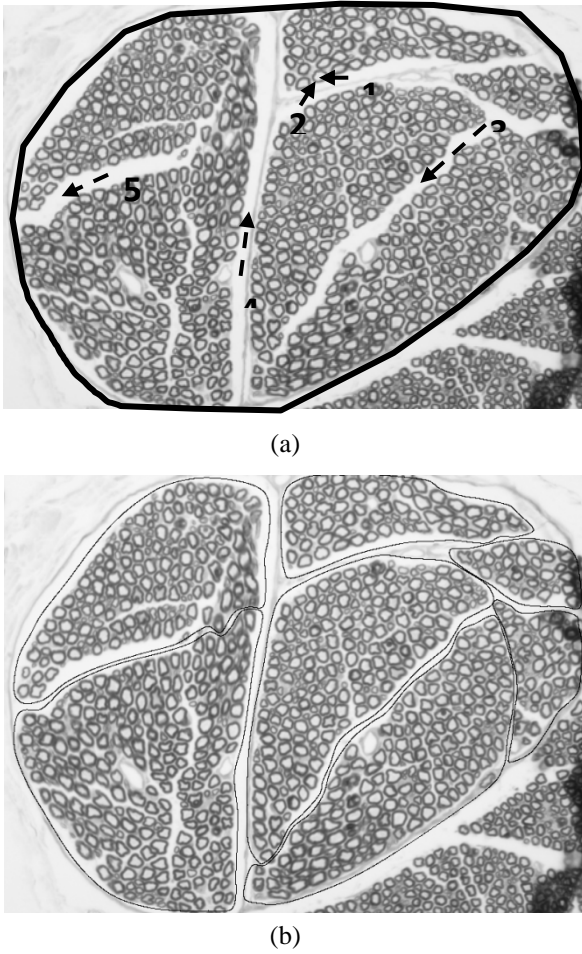


Figure 1: Example of a myelinated nerve fiber cross-sectional image: (a) a cross section of a myelinated nerve fiber. Arrow 1 points out an axon, and arrow 2 indicates its myelin sheath. A nerve fascicle is bounded by a continuous membrane as drawn in the black thick contour. The fascicle is divided into several sub-fascicles (as indicated by arrows 3–5) due to natural crack-like separations. (b) The manually drawn boundaries of each sub-fascicle.

3. Method

Segmentation and reconstruction of a 3D structure of nerve fiber are rather complicated because each microscopic cross-sectional image contains an enormous number of MNFCs while the MNFCs' intensity appearances and positions are usually inconsistent between different cross sections. The proposed method combines image processing techniques, watershed segmentation and point registration algorithms to cope with these difficulties. Given a sequence of nerve fiber microscopic cross sections, we first adopt a single-frame watershed-based segmentation algorithm to segment

MNFCs from each microscopic image. Next, we propose the SCR strategy to sequentially align each pair of adjacent image frames and establish the connectivity of inter-frame MNFCs. At last, a compensation mechanism is developed to recover the missing MNFCs. The 3D structure of nerve fiber can consequently be reconstructed based on the segmentation results for MNFCs.

3.1 MNFC Segmentation from Each Individual Cross-sectional Image

A method that mainly utilizes the multi-level gradient watershed scheme associated with three fuzzy systems is applied to each individual cross-sectional image for automatic segmentation of MNFCs. Since this method refers to our previous study [4], we only give a brief introduction here. In the multi-level gradient watershed scheme, pre-candidate MNFCs at each immersion level are extracted and then examined by the first fuzzy rule system with certain conditions. If the fuzzy output meets certain conditions, the pre-candidate MNFCs are accepted as candidates. The second fuzzy system is then used to obtain the parameters of a rule-based active contour model for the refinement of boundaries of the MNFC candidates. Finally, the third fuzzy rule system based on the intensity and geometric characteristics of MNFCs is used to confirm if these candidates are true MNFCs or not. By applying the flexibility in the multi-scale watershed and the knowledge embedded in fuzzy rule systems, we can successfully handle the complications inherent in automatic segmentation of the MNFCs from each individual frame.

3.2 Spatially Constrained Registration (SCR) Strategy

Considering that the 2D watershed algorithm may mis-segment some MNFCs with vague boundaries or irregularly distribute intensities, we thus propose a SCR strategy to correlate inter-frame MNFCs in order to improve the segmentation results. As a full nerve fascicle is usually composed of several sub-fascicles, and each sub-fascicle is located with an individual geometric transformation, it is difficult to use only a global geometric transformation for characterizing the spatial relationship of the entire nerve fascicle between adjacent frames. The proposed SCR strategy resolves this difficulty by first globally aligning the full-fascicle cross sections on adjacent frames by the ICP algorithm, and then individually registering sub-fascicle cross sections by a new spatially constrained point registration (SCPR) is approached.

3.2.1 Full-fascicle Registration by ICP

We first utilize the Canny edge detector to extract notable edges from each image frame. Then we adopt the ICP algorithm to register the edge points on two adjacent frames. Given a source point set $\mathbf{S} = \{\mathbf{s}_i\}_{i=1}^{N_s}$ and a target point set $\mathbf{M} = \{\mathbf{m}_j\}_{j=1}^{N_m}$, the ICP finds a rigid transformation \mathbf{T} that best aligns \mathbf{S} to \mathbf{M} , where N_s and N_m denote the numbers of source and target points, respectively. The transformation \mathbf{T} is solved via an iterative optimization process based on the least square criterion:

$$\min_{\mathbf{T}, j(i) \in \{1, 2, \dots, N_m\}} \sum_{i=1}^{N_s} \|\mathbf{T}(\mathbf{s}_i) - \mathbf{m}_{j(i)}\|^2 \quad (1)$$

Since a rigid transformation can be decomposed into a rotation matrix \mathbf{R} and a translation vector \mathbf{t} , Eq. (1) is rewritten as:

$$C_k(i) = \arg \min_{j(i)} \|\mathbf{R}_k \cdot \mathbf{s}_i + \mathbf{t}_k - \mathbf{m}_{j(i)}\|^2, \quad i \in \{1, 2, \dots, N_s\}, j(i) \in \{1, 2, \dots, N_m\}. \quad (3)$$

Note that, the transformation matrix at the first iteration is initialized as an identity matrix. Next, the rotation and translation $(\mathbf{R}_{k+1}, \mathbf{t}_{k+1})$ at the $(k+1)$ -th

$$(\mathbf{R}_{k+1}, \mathbf{t}_{k+1}) = \arg \min_{\mathbf{R}'_k, \mathbf{t}'_k} \sum_{i=1}^{N_s} \|\mathbf{R}'_k \cdot \mathbf{s}_i + \mathbf{t}'_k - \mathbf{m}_{C_k(i)}\|^2, \quad \mathbf{R}'_k{}^T \mathbf{R}'_k = \mathbf{I}_m, \det(\mathbf{R}'_k) = 1. \quad (4)$$

After the ICP registration process, the adjacent image frames can be globally aligned by using the resulting registration parameters (i.e., rotation and translation).

On the other hand, to capture the spatial offsets of sub-fascicles between different image frames, we have to delineate the sub-fascicle boundaries from each frame. In the proposed method, each sub-fascicle contour on the first frame is outlined manually and then propagated sequentially to all the other frames. The MNFCs enclosed by the sub-fascicle contour are then regarded as in the same group. Occasionally, different sub-fascicles may be very close and have ambiguous boundaries (arrows in Fig. 1(b)), so visual examination and manual adjustments are needed to assure the partitions. After finishing the contour propagation from the first frame to the last, the partitions of sub-fascicles on each frame can be obtained.

$$\min_{\mathbf{R}, \mathbf{t}, j(i) \in \{1, 2, \dots, N_m\}} \sum_{i=1}^{N_s} \|\mathbf{R} \cdot \mathbf{s}_i + \mathbf{t} - \mathbf{m}_{j(i)}\|^2, \quad \mathbf{R}^T \mathbf{R} = \mathbf{I}_m, \det(\mathbf{R}) = 1. \quad (2)$$

An efficient method to solve the transformation parameters in Eq. (2) was suggested by Besl and McKay [17]. Two processing steps are used to register the source data to the target. The first step is to find the correspondence between two point sets, and the second step is to calculate the transformation parameters, \mathbf{R} and \mathbf{t} . For the i -th point of source data \mathbf{S} , its corresponding point in target data \mathbf{M} , denoted as $C_k(i)$ where k is the index of iteration, can be obtained based on the rigid transformation $(\mathbf{R}_k, \mathbf{t}_k)$ between \mathbf{S} and \mathbf{M} :

iteration are updated based on the correspondent $\{(i, C_k(i))\}_{i=1}^{N_s}$:

3.2.2 Sub-fascicle Registration by SCPR

This registration step aims at registering the MNFCs of the same sub-fascicle from frame u to frame $u + 1$, and also at establishing the connectivity between inter-frame MNFCs. Since the ICP algorithm identifies point correspondences only based on the Euclidean distance, it tends to yield incorrect MNFC correspondences so to establish unreliable inter-frame MNFC connectivity. The proposed point registration method, i.e. SCPR, is utilized to handle this problem and achieve the sub-fascicle registration. First, for each MNFC on frame u , we calculate three geometric features which indicate the fitness of correspondences with respect to the neighboring MNFCs on frame $u + 1$. Second, we establish the correspondences of MNFCs on frames u and frame $u + 1$ based on the inferring result of the fuzzy system whose inputs are the calculated features. Third, we solve the rigid transformation of the sub-fascicle by maximizing the sum of fuzzy values from all pairs of corresponding MNFCs. These three steps are iteratively performed until the difference between the transformations obtained in the current and previous iterations is smaller than a predefined threshold.

3.2.2.1 Calculating Geometric Features of MNFCs

Let the MNFCs on frames u and $u + 1$ denote the source and target point sets \mathbf{S} and \mathbf{M} , respectively. Given two MNFCs, i.e., \mathbf{s}_i and \mathbf{m}_j , the geometric features including overlapping ratio, center distance and neighborhood structural similarity are calculated.

- 1). *Overlapping ratio between MNFCs.* The first feature is the overlapping ratio, which measures the spatial dependency between two MNFC regions on adjacent frames:

$$\text{Overlapping region ratio} = \frac{\mathbf{O}(\mathbf{s}_i) \cap \mathbf{O}(\mathbf{m}_j)}{\mathbf{O}(\mathbf{s}_i) \cup \mathbf{O}(\mathbf{m}_j)} \quad (5)$$

where $\mathbf{O}(\mathbf{s}_i)$ is the i -th MNFC region on frames u , and $\mathbf{O}(\mathbf{m}_j)$ is the j -th MNFC region on frames $u + 1$. The value of this ratio should be high if the two MNFCs correspond with each other.

- 2). *Center distance.* The second feature which measures the distance between the centers of two MNFCs is defined as

$$\text{Distance} = \|\mathbf{s}_i - \mathbf{m}_j\| \quad (6)$$

where \mathbf{s}_i represents the coordinate of center of the i -th MNFC on frame u , and \mathbf{m}_j represents the coordinate of center of the j -th MNFC on frame $u + 1$. A pair of better corresponding MNFCs presents a smaller distance value.

- 3). *Neighborhood structural similarity of MNFCs.* The third feature is the neighborhood structural similarity between two MNFCs. At first, we build the Voronoi diagram [24] to characterize the spatial relationship of the neighborhood of each MNFC on the image frame, as shown in Fig. 2(a). The centers of the MNFCs are indicated by the red points; their contours obtained from the watershed segmentation are in green, and the resulting Voronoi regions are separated with the red lines. For each MNFC, its neighbors can then be specified by the adjacent Voronoi regions. Next, a triangulation process, in which the

$$\text{Neighborhood structure similarity} = \sum_{a \in \text{Nei}(i), b \in \text{Nei}(j)} \left\| (\mathbf{s}_i - \mathbf{s}_a) - (\mathbf{m}_j - \mathbf{m}_b) \right\| \quad (7)$$

where \mathbf{s}_i represents the coordinate of center of the i -th MNFC, and \mathbf{s}_a represents the coordinate of center of the a -th neighbor of the i -th MNFC on frame u . \mathbf{m}_j represents the coordinate of center of the j -th MNFC, and \mathbf{m}_b represents the coordinate of center of the

centers of neighboring MNFCs are connected to each other, is carried out for the purpose of describing the neighborhood structure. Its implementation details can be referred to the Delaunay triangulation method [25]. Fig. 2(b) shows the resulting triangular mesh (as indicated by the blue lines), where each vertex represents a MNFC's center. The direction and length of its one-ring edges are then used to describe the spatial relationship with respect to the neighbors.

With the triangular meshes of MNFCs on frames u and $u + 1$, the third feature value is calculated by

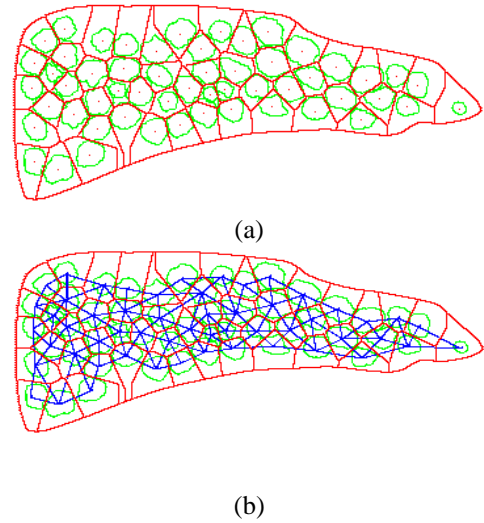


Figure 2: Illustrations for Voronoi diagram (a), and triangular mesh (b) in a sub-fascicle. The red dots in (a) indicate the centers of MNFCs, and the green contours outline the MNFC regions. The red lines show the Voronoi diagram constructed from the MNFCs. The triangular mesh in (b) is shown with the blue lines.

b -th neighbor of the j -th MNFC on frame $u + 1$. In the implementation, we at first utilized the ICP algorithm to align the neighbors of \mathbf{s}_i and \mathbf{m}_j to obtain their one-ring neighbor correspondences for the calculation of Eq. (7). Here, \mathbf{m}_b is the closest point of \mathbf{s}_a on frame $u +$

1 after the alignment. Consequently, we can measure the similarity of spatial distributions of neighbors for the MNFCs on adjacent frames. The fitness of better correspondence of MNFCs can be reflected in a smaller value for the structural similarity feature.

3.2.2.2 Establishing Correspondence Based on Fuzzy Inference

In this section, we illustrate how the three features are integrated by the fuzzy inference system to establish the correspondences of MNFCs for the registration process. A fuzzy

if-then rule is expressed as “if x is A, then y is B, where A and B are fuzzy subsets.” In our proposed SCPR method, there are two levels for describing each feature value, and thus, totally there are eight rules to be hired, as summarized in Table I. For example, rule 1 means: if the overlapping ratio is high, the center distance is small, and the structural similarity value is also small, so the fitness of the correspondence is high.

We use the Zadeh’s method [26] to infer the rules as

Table 1: Fuzzy rules used to define fuzzy value.

Rule 1	If (O is High) \wedge (D is Short) \wedge (S is Small)	Then B(y) is High
Rule 2	If (O is High) \wedge (D is Short) \wedge (S is Large)	Then B(y) is Low
Rule 3	If (O is Low) \wedge (D is Short) \wedge (S is Small)	Then B(y) is Low
Rule 4	If (O is Low) \wedge (D is Short) \wedge (S is Large)	Then B(y) is Low
Rule 5	If (O is High) \wedge (D is Long) \wedge (S is Small)	Then B(y) is Low
Rule 6	If (O is High) \wedge (D is Long) \wedge (S is Large)	Then B(y) is Low
Rule 7	If (O is Low) \wedge (D is Long) \wedge (S is Small)	Then B(y) is Low
Rule 8	If (O is Low) \wedge (D is Long) \wedge (S is Large)	Then B(y) is Low

O = overlapping ratio, D = center distance, S = structure similarity value

$$B'(y) = \min_{r=1}^8 \left\{ \max[A_1^r(O) \wedge A_2^r(D) \wedge A_3^r(S) \wedge B^r(y), 1 - [A_1^r(O) \wedge A_2^r(D) \wedge A_3^r(S)]] \right\} \quad (8)$$

where A_1 , A_2 and A_3 are the membership functions of the three features, respectively, and B is the output of the fuzzy system. The O, D and S note the overlapping ratio, center distance and neighborhood structural similarity value, respectively. The corresponding fuzzy sets A_1 , A_2 , A_3 and B are

illustrated in Fig. 3. Here, we denote $B'(y)$ as the inferring result that minimizes the integrated value of the eight given fuzzy rules. As a result, the fuzzy value (FV) can be obtained by computing the center of gravity of $B'(y)$, which is the integrated measurement of the three geometric features.

Degree of membership
function

Level 1 Level 2

Membership function

Variable	Membership function	Level 1	Level 2
Overlapping ratio (O)	A ₁	low	high
Distance between centers (D)	A ₂	short	long
Structural similarity value (S)	A ₃	small	large
Output value: The prob. of being a correspondence (y)	B	low	high

Figure 3: Fuzzy membership functions for overlapping ratio / distance between centers / structural similarity value / output value.

In the registration process of MNFC sets \mathbf{S} and \mathbf{M} on frames u and $u + 1$, the transformation matrix at the first iteration is initialized by an identity matrix. For the i -th MNFC on frame u , in order to find its best correspondence, we have to first include some candidates on frame $u+1$ for the calculation of FVs. The candidates are determined as the closest MNFC and all its neighbors. Then the

correspondences $\{(i, C_k(i))\}_{i=1}^{N_s}$ at the k -th iteration can be obtained based on the rigid transformation $(\mathbf{R}_k, \mathbf{t}_k)$:

$$C_k(i) = \arg \max_{j(i)} \{FV_{i,j(i)}((\mathbf{R}_k \cdot \mathbf{s}_i + \mathbf{t}_k), \mathbf{m}_{j(i)}), j(i) \in \{1, 2, \dots, N_m\}\} \quad (9)$$

where $FV_{i,j(i)}$ represents the fuzzy value calculated from the i -th MNFC on frame u and the $j(i)$ -th MNFC on frame $u+1$. The fitness of the correspondence is indicated by the FV, and the candidate with the maximal FV is finally selected as the best corresponding MNFC with respect to \mathbf{s}_i .

3.2.2.3 Solving the Registration Transformation

After establishing the correspondences of MNFCs between frames u and $u + 1$, the registration transformation is then updated. At the $(k+1)$ -th iteration, the rotation and translation $(\mathbf{R}_{k+1}, \mathbf{t}_{k+1})$ are updated based on the correspondences $\{(i, C_k(i))\}_{i=1}^{N_s}$ estimated from the k -th iteration:

$$(\mathbf{R}_{k+1}, \mathbf{t}_{k+1}) = \arg \max_{\mathbf{R}'_k, \mathbf{t}'_k} \sum_{i=1}^{N_k} \text{FV}_{i,C_k(i)}, \quad \mathbf{R}'_k{}^T \mathbf{R}'_k = \mathbf{I}_m, \quad \det(\mathbf{R}'_k) = 1 \quad (10)$$

where $\text{FV}_{i,C_k(i)}$ is the fuzzy value calculated from a pair of corresponding MNFCs at the k -th iteration. Eq. (10) is used to solve the optimal rigid transformation by maximizing the sum of FVs, which indicates the fitness of MNFC correspondences. Through the iterative three-step optimization procedure, the proposed SCPR can achieve the registration of sub-fascicles between arbitrary two adjacent frames.

3.3 Compensation Mechanism for Recovering Missing MNFCs

The previous watershed segmentation, however, may miss some MNFCs due to the artifacts of specimen slicing or imaging, as exemplified in Fig. 4. Three sequential frames containing two MNFCs (a and b) are illustrated; MNFC a is successfully detected on all the three frames. However, MNFC b is detected only on frames 1 and 3, and is missed on frame 2. To deal with the situation as MNFC b , we thus design the compensation mechanism based on MNFC connectivity to recover the missing MNFCs.

The compensation mechanism includes two stages, which are a dummy MNFC creation and validation. In the creation stage, if an MNFC on frame u does not have a corresponding MNFC on frame $u+1$, then a dummy MNFC is created and is placed on frame $u+1$ (d_MNFC_{u+1}). Note that, if there is no MNFC on frame $u+1$ in an area fifteen pixels from the corresponding center of a MNFC on frame u , it is classified as the one without correspondence. In the given example, we hence create a dummy MNFC b on frame 2 based on the registration transformation between frame 1 and frame 2. In the validation stage, the MNFC on frame $u+2$ is backward mapped to frame $u+1$, and a dummy MNFC ($d_MNFC'_{u+1}$) is thus created in a similar way. The existence of this dummy MNFC is considered valid if the overlapping ratio of d_MNFC_{u+1} and $d_MNFC'_{u+1}$ is larger than a predefined threshold (0.8 in the experiments), which is discarded otherwise. The center of the valid dummy MNFC on frame $u+1$ is given by the average of center positions of d_MNFC_{u+1} and $d_MNFC'_{u+1}$. Its contour is specified by the average shape of d_MNFC_{u+1} and $d_MNFC'_{u+1}$. Consequently, we are able to regain the missing MNFCs based on the compensation mechanism that takes the inter-frame MNFC connectivity into account.

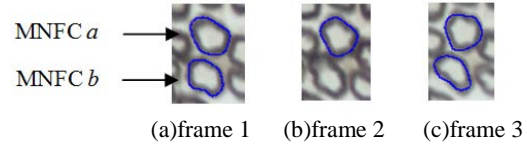


Figure 4: Example of mis-segmentation of MNFC: (a)-(c) represent three consecutive frames. MNFC a is successfully segmented on the three frames; however, MNFC b is missed on the intermediate frame.

Since there are certain shape deviations between the valid dummy MNFCs and the image, we hence employ the active contour model (ACM) algorithm [27] to refine the shapes of the dummy MNFCs to better fit the true boundaries on frame $u+1$. The contour of each valid dummy MNFC serves as the initial of the ACM. The ACM deformation that iteratively adjusts the contour points toward the true MNFC boundaries is achieved by minimizing the following energy function:

$$E_{ACM} = \int_0^1 (E_{internal}(v(s)) + E_{external}(v(s))) ds \quad (11)$$

where $v(s)$ represents the coordinate of a point on the contour model; $E_{internal}$ is the internal energy and $E_{external}$ is the external energy.

The internal energy, which is used to control the continuity and smoothness of the model boundary, is formulated as

$$E_{internal}(v(s)) = \frac{|v'(s)|^2 + |v''(s)|^2}{s_m}, \quad (12)$$

where s_m is a constant for normalization, and $v'(s)$ and $v''(s)$ are the first and second derivatives of the contour model, representing the continuity and curvature at $v(s)$, respectively. As the MNFCs are supposed to be smooth and circular in shape, the internal energy can be used to avoid unreasonable model distortions and maintain shape smoothness during the deformation process. On the other hand, the external energy used to attract the model to the MNFC boundaries is defined as

$$E_{external}(v(s)) = \frac{\nabla I(v(s))}{I_{max} - I_{min}}, \quad (13)$$

where $\nabla I(v(s))$ indicates the gradient component of intensity of $v(s)$ along the outward-pointing normal of the model boundary. I_{max} and I_{min} represent the maximal and minimal intensities along the normal, respectively, and their difference is used as a normalization term. The external energy is used to capture the MNFC boundaries, which are expected to appear in the transition from low to high intensity. After the compensation process is accomplished, we are able to reconstruct the 3D structure of nerve fiber based on a consecutive sequence of segmented MNFCs, as shown in Fig. 5.

(a)

(b)

Figure 5: Reconstruction results of 3D structure of the nerve fibers segmented from two different image sequences.

4. Results and Discussion

The following experiments include accuracy and performance evaluations. The evaluation works were achieved by applying the proposed segmentation algorithm to two microscopic imagesets

of rat tibia nerves, one of which consists of eight image frames, and the other of which contains five ones. The two nerve image sets contain five and one sub-fascicles, respectively. As different sub-fascicles in the same nerve fiber may still have their own biological characteristics and show respective intensity variations, the number of experiment samples (5 sub-fascicles \times 8 cross sections + 1 sub-fascicle \times 5 cross sections) should be acceptable. Two experts were consulted to obtain the ground truth manually in the validation experiments. The MNFCs, which were less than ten pixels in area or had boundaries that were too vague, were excluded in the experiments.

4.1 Accuracy Evaluation of The Proposed Method

The aim of this experiment was to evaluate the detection rate of MNFCs obtained by the proposed registration-based segmentation method. The detection rate was defined as the ratio of number of true positive MNFCs to the total number of the ground truth, which was obtained from the manual detection results from two experts. For each intermediate frame of the image sequence (i.e., excluding the first and last frames), we measured the detection rate of MNFCs from each sub-fascicle and then averaged the detection rates of each sub-fascicle for all images. The averaged detection rate for each sub-fascicle is shown in Table 2. Overall, the proposed method achieved a very high detection rate of 91.8%. Compared to the results (around 93.3%) of Fok's work [28], which segmented the nerve fibers of human brain, our method shows comparable results. Moreover, the number of MNFCs they handled in each image was smaller than fifty, which is considerably less than ours with several hundreds of MNFCs in each image. As a whole, the proposed method not only shows great accuracy with regard to MNFC segmentation, but also demonstrates a good capability of handling the segmentation of a large number of MNFCs.

Table 2: Accuracy evaluation of the proposed method.

		Averaged detection rate (%)
Image sequence 1	Sub-fascicle 1 (8 cross sections)	89
	Sub-fascicle 2 (8 cross sections)	93
	Sub-fascicle 3 (8 cross sections)	91
	Sub-fascicle 4 (8 cross sections)	93
	Sub-fascicle 5 (8 cross sections)	92
Image sequence 2	Sub-fascicle 1 (5 cross sections)	93
Std.		1.62
Mean		91.8

4.2 Performance Evaluation of the Proposed Method

4.2.1 Correctness of MNFC Correspondences

In this experiment, a comparison study was carried out to evaluate how the proposed SCPR method can establish more reliable MNFC correspondences over the conventional ICP algorithm. We examined the correctness of MNFC correspondences obtained by the two registration methods referenced above. A quantitative evaluation was achieved by calculating the correspondence correctness ratio (CCR), which is obtained by dividing the number of true positive correspondences (NTPC) by the number of true correspondences (NTC). The NTC represents the number of true correspondences between MNFC pairs, inspected manually by the experts referred above. The NTPC is the number of MNFC correspondences of the automatic detection results which are consistent with the correspondences of

ground truth. A higher value of CCR indicates a better accuracy and reliability of correspondence establishment.

There were five and one sub-fascicles in image sequences 1 and 2, respectively. Performances of the proposed SCPR and the conventional ICP methods were evaluated by calculating the CCR of the sub-fascicle on all adjacent frames. The evaluation results are listed in Table 3, in which the average CCR of the proposed method shows superiority over the conventional ICP. Such an improvement is because the proposed method utilizes multiple spatial features, including overlapping ratios, center-to-center distance, and neighborhood structural similarity, with regard to searching for the correspondences of MNFCs, whereas the conventional ICP takes only the closest point distances into account.

Table 3: Performance comparison between the proposed SCPR and conventional ICP by correspondence correctness ratio (CCR).

		CCR obtained by SCPR (%)	CCR obtained by conventional ICP (%)
Image sequence 1	Sub-fascicle 1 (8 cross sections)	88	85
	Sub-fascicle 2 (8 cross sections)	92	90
	Sub-fascicle 3 (8 cross sections)	95	93
	Sub-fascicle 4 (8 cross sections)	94	90
	Sub-fascicle 5 (8 cross sections)	94	78
Image sequence 2	Sub-fascicle 1 (5 cross sections)	93	89
	Std.	2.50	5.32
	Mean	92.6	87.5

4.2.2 Recovery rate of missing MNFCs

In this experiment, we illustrated how the proposed registration-based segmentation method can improve the MNFC segmentation results, which were obtained by the single-frame watershed-based method from our preliminary study [4]. At first, we demonstrated an example in Fig. 6 for illustrating the effectiveness of the proposed idea in recovering the missing MNFCs. As shown in this figure, using the previously developed method can achieve good segmentations for most MNFCs. However, certain artifacts in the specimen slicing process will lead to vague MNFC boundaries (as indicated in the middle part of Fig. 6(b)), making the pure 2D watershed segmentation prone to mis-detections. After the proposed MNFC compensation process, we recovered 16 missing MNFCs (around 78%) as shown in Fig. 6(c). Obviously, the final segmentation result obtained by the proposed registration-based method seen in Fig. 6(d) has been much improved over the original seen in Fig. 6(b).

Beyond the qualitative demonstration, we also evaluated the recovery performance via a quantitative experiment. We defined a recovery rate as the ratio of number of successfully recovered MNFCs to the number of missing MNFCs in a sub-fascicle. For each intermediate frame in the image sequence, i.e., excluding the first and last frames, the recovery rate could be calculated. For the five sub-fascicles, the average recovery rates of the six intermediate frames on the first image sequence were 65%, 32%, 62%, 56% and 76%, respectively. The average recovery rate of the three intermediate frames in the second image sequence was 71.5%. The improvement of the segmentation results after the recovery process was notable. Therefore, the performance of the proposed compensation mechanism has been confirmed in some sense.

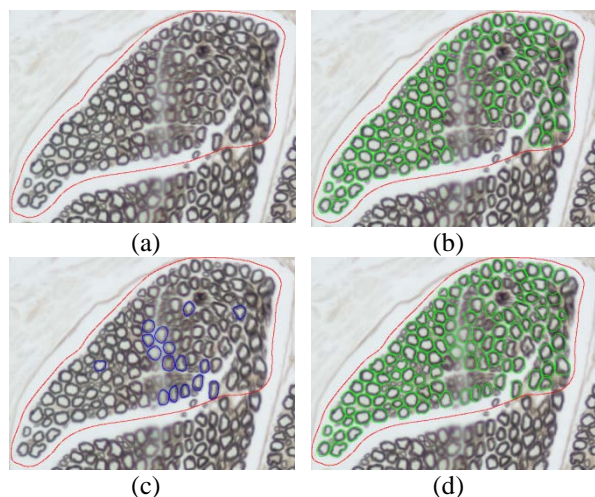


Figure 6: Performance evaluation of the proposed method: (a) MNFCs of a sub-fascicle in the original image; (b) the segmentation result for a purely 2D multi-scale watershed [4]; (c) the recovery results for MNFCs (blue) by using the proposed registration-based segmentation; (d) the final segmentation result for MNFCs.

5. Conclusion

In this paper we proposed an inter-frame registration-based segmentation method by which to obtain the 3D structure of nerve fiber from sequential microscopic cross-sectional images. The proposed method first segmented the MNFCs from each single image frame by using the multi-scale watershed hierarchical approach. Then we designed the spatially constrained registration (SCR) strategy, which takes image, geometric and biological structural features of MNFCs into account in order to register adjacent image frames and obtain the correspondences of inter-frame MNFCs. With the established connectivity, the proposed compensation mechanism efficiently recovered the missing MNFCs, certainly improving the segmentation results. The experimental results showed that the proposed method is more reliable on correspondence establishment than the ICP algorithm. Moreover, it achieved high segmentation accuracy with a detection rate of 91%. In the future, the proposed method can be applied to solve other image segmentation problems with a large number of cellular objects. Our system, which is near fully-automatic, can also help clinicians or researchers to efficiently collect reproducible data for investigating cell mechanics and evaluating neurological disorders.

Acknowledgment

The authors would like to express their appreciation for the grant under contract NSC 98-2221-E-006-140-MY3 from the National Science Council, Taiwan, R.O.C.. Also, this work made use of shared facilities supported by the Program of Top 100 Universities Advancement, Ministry of Education, Taiwan, R.O.C..

References

- [1]. Y. Al-Kofahi, W. Lassoued, W. Lee, B. Roysam, Improved automatic detection and segmentation of cell nuclei in histopathology images, *IEEE Trans. Biomed. Eng.* 57(4)(2010) 841–852.
- [2]. X.Zhou, F.Li, J.Yan, S.T.Wong, A novel cell segmentation method and cell phase identification using Markov model, *IEEE Trans. Inf. Technol. B.* 13(2) (2009) 152–157.
- [3]. J.Cheng, J.C.Rajapakse, Segmentation of clustered nuclei with shape markers and marking function, *IEEE Trans. Biomed. Eng.* 56(3)(2009) 741–748.
- [4]. Y.Y.Wang, Y.N.Sun, C.C. K.Lin, M.S.Ju, Segmentation of nerve fibers using multi-level gradient watershed and fuzzy systems, *Artif. Intell. Med.* (2012) In Press.
- [5]. C.Zanella, M.Campana, B. Rizzi, C. Melani, G.Sanguinetti, P.Bourgine, K.Mikula, N.Peyrieras, A.Sarti, Cells segmentation from 3-D confocal images of early zebrafish embryogenesis, *IEEE Trans. Image Process.* 19(3) (2010) 770–781.
- [6]. B.C.Ko, M.S.Seo, J.Y. Nam, Microscopic cell nuclei segmentation based on adaptive attention window, *J. Digit. Imaging* 22(3)(2008) 259–274.
- [7]. K.Althoff, J.Degerman, T.Gustavsson, Combined segmentation and tracking of neural stem-cells, *Lecture Notes in Computer Science* 3540 (2005) 282–291.
- [8]. M.E. Plissiti, C.Nikou, A.Charchanti, Combining shape, texture and intensity features for cell nuclei extraction in Pap smear images, *Pattern Recogn.Lett.* 32 (2011) 838–853.
- [9]. F.B.Tek, A.G.Dempster, I. Kale, Blood cell segmentation using minimum area watershed and circle radon transformations, *Computational Imaging and Vision* 30 (2004) 441–454.
- [10]. J.Kan, Q.M.Liao, X.Yuan, A novel white blood cell segmentation scheme based on feature space clustering. *Soft Comput.* 10 (2006) 12–19.

- [11]. S.Colantonio, O. Salvetti, I.B. Gurevich, A two-step approach for automatic microscopic imagesegmentation using fuzzy clusteringand neural discrimination, *Pattern Recogn. Image Anal.*17(3)(2007)428–437.
- [12]. A.F.Frangi, D.Rueckert, J.A.Schnabel, W.J.Niessen, Automatic construction of multiple-object three-dimensional statistical shape models: application to cardiac modeling,*IEEE Trans. Med. Imag.*21(9)(2002) 1151–1166.
- [13]. A.Yezzi, L.Zollei, T.Kapur, A variational framework for integrating segmentation and registration through active contours, *Med. Image Anal.*7 (2003)171–185.
- [14]. S.Gorthi, V.Duay, N.Houhou, M. Bach Cuadra, U. Schick, M. Becker, A. S.Allal, J. Thiran, Segmentation of head and neck lymph node regions for radiotherapy planning, using active contour based atlas registration,*IEEE J. Sel. Topics Signal Process.*3(1)(2009) 135–147.
- [15]. H.C.Chen, I.M. Jou, C.K.Wang, F.C.Su, and Y.N. Sun, Registration-based segmentation with articulated model from multipostural magnetic resonance images for hand bone motion animation, *Med. Phys.*37(2010) 2670–2682.
- [16]. V.Zagrodsky, V. Walimbe, C.R.Castro-Pareja, J.X. Qin, J.M. Song, R.Shekhar, Registration-assisted segmentation of real-time 3-D echocardiographic data using deformable models, *IEEE Trans. Med. Imag.* 21 (9)(2005) 1089–1099.
- [17]. P.J.Besl,N.D.McKay,A method for registration of 3D shapes, *IEEE Trans. Pattern Anal. Mach. Intell.* 14(2)(1992) 239–256.
- [18]. L.Zhang, S.I.Choi, S.Y.Park, Robust ICP registration using biunique correspondence,in *International Conference on 3D Imaging, Modeling, Processing, Visualization and Transmission*, 2011, pp. 80–85.
- [19]. M.Rogers, J. Graham, Robust and accurate registration of 2-D electrophoresis gels using point-matching, *IEEE Trans. on Image Processing*16(3)(2007) 624–635.
- [20]. G.C.Sharp, S.W. Lee, D.K. Wehe, ICP registration using invariant features, *IEEE Trans. Pattern Anal. Mach. Intell.* 24(1)(2002) 90–102.
- [21]. F.L.Chung, Z. Deng, S. Wang, An adaptive fuzzy-inference-rule-based flexible model for automatic elastic image registration,*IEEE Trans. Fuzzy Systems* 17(5)(2009) 995–1010.
- [22]. S.Kobashi, Y. Fujiki, M. Matsui, N. Inoue,K. Kondo, Y. Hata, T. Sawada, Interactive segmentation of the cerebral lobes with fuzzy inference in 3T MR images,*IEEE Trans. Syst. Man, Cy. B.* 36(1)(2006) 74–86.
- [23]. X.Chen, J.Tian, X.Yang,Anew algorithm for distorted fingerprints matching based on normalized fuzzy similarity measure, *IEEE Trans. Image Process.*15(3)(2006) 767–776.
- [24]. L.Guibas, J.Stolfi, Primitives for the manipulation of general subdivisions and the computations of voronoidiagrams,*ACM Trans. Graphics*4 (1985) 74–123.
- [25]. J.Krämer, Delaunay triangulation in two and three dimensions,*Master's thesis*, Wilhelm Schickard Institute for Computer Science Graphical-Interactive Systems, University of Tübingen (1995).
- [26]. L. A.Zadeh,J. Kacprzyk,*Fuzzy Logic for the Management of Uncertainty*. John Wiley & Sons, Inc., New York, NY, USA.
- [27]. M.Kass, A.Witkin, D. Terzopoulos,Snake: active contour models, *Int. J. Comput. Vis.* 1(4)(1988) 321–331.
- [28]. Y.L.Fok, J.C.K. Chan, R.T.Chin, Automated analysis of nerve-cell image using active contour models, *IEEE. Trans. Med. Imaging*15(3)(1996) 353–368.